

Experimental study of the interfacial cobalt oxide in $\text{Co}_3\text{O}_4/\alpha\text{-Al}_2\text{O}_3(0001)$ epitaxial films

C. A. F. Vaz,^{1,2,*} D. Prabhakaran,³ E. I. Altman,^{4,2} and V. E. Henrich^{1,2}

¹*Department of Applied Physics, Yale University, New Haven, Connecticut 06520*

²*Center for Research on Interface Structures and Phenomena (CRISP),
Yale University, New Haven, Connecticut 06520*

³*Department of Physics, Clarendon Laboratory, Oxford University, Oxford OX1 3PU, United Kingdom*

⁴*Department of Chemical Engineering, Yale University, New Haven, Connecticut 06520*

(Dated: October 14, 2009)

A detailed spectroscopic and structural characterization of ultrathin cobalt oxide films grown by O-assisted molecular beam epitaxy on $\alpha\text{-Al}_2\text{O}_3(0001)$ single crystals is reported. The experimental results show that the cobalt oxide films become progressively more disordered with increasing thickness, starting from the early stages of deposition. Low energy electron diffraction patterns suggest that the unit cell remains similar to that of $\alpha\text{-Al}_2\text{O}_3(0001)$ up to a thickness of 17 Å, while at larger thicknesses a pattern identified with that of $\text{Co}_3\text{O}_4(111)$ becomes visible. X-ray photoelectron spectroscopy reveals sudden changes in the shape of the Co 2p lines from 3.4 to 17 Å cobalt oxide thickness, indicating the transition from an interfacial cobalt oxide layer towards [111]-oriented Co_3O_4 . In particular, the absence of characteristic satellite peaks in the Co 2p lines indicates the formation of a trivalent, octahedrally coordinated, interfacial cobalt oxide layer during the early stages of growth, identified as the Co_2O_3 corundum phase.

PACS numbers: 68.37.-d, 68.35.Ct, 68.37.Og, 68.37.Ps, 68.55.-a, 75.50.Ee

I. INTRODUCTION

The stability of polar surfaces, characterized by a net surface charge, has long been a topic of much interest, since the large electrostatic energies associated with such surfaces are expected to lead to modified electronic and atomic structures, with attendant changes in physical properties.^{1,2,3} This often leads to surface structures that depart significantly from a simple truncation of the bulk crystal, exhibiting reconstructions, faceting, surface roughening, altered valencies,^{2,3,4,5,6,7,8,9,10,11} and that can give rise to other exotic phenomena, such as the onset of two-dimensional metallic states in $\text{LaAlO}_3/\text{SrTiO}_3(001)$ interfaces.^{12,13}

Recently, we reported the epitaxial growth of $\text{Co}_3\text{O}_4(110)/\text{MgAl}_2\text{O}_4(110)$ and $\text{Co}_3\text{O}_4(111)/\alpha\text{-Al}_2\text{O}_3(0001)$ thin films, which were found to exhibit (1×1) surfaces, despite the fact that both surfaces are polar; while the as-grown film surfaces show some degree of disorder, annealing in air results in atomically smooth films for $\text{Co}_3\text{O}_4(110)$, and improved morphology for the $\text{Co}_3\text{O}_4(111)$ films, while retaining the (1×1) surface structure.^{10,11} The stability of these surfaces was attributed to a modified surface valency of the Co cations, corresponding effectively to a surface inversion in the spinel structure; identical conclusions were reached in a study of the growth of twinned (1×1) [111]-oriented Co_3O_4 films on $\text{Ir}(001)-(1 \times 1)$,⁹ and in $\text{Fe}_3\text{O}_4(111)/\text{Pt}(111)$ thin films, which also exhibit a (1×1) surface.⁶ One unresolved issue remains the interface structure at the early stages of growth of $\text{Co}_3\text{O}_4(111)/\alpha\text{-Al}_2\text{O}_3(0001)$. The observation of a significant amount of disorder occurring at the $\text{Co}_3\text{O}_4/\alpha\text{-Al}_2\text{O}_3(0001)$ interface was tentatively attributed to the

possibility of the formation of an off-stoichiometric cobalt oxide, perhaps closer to the corundum Co_2O_3 phase. In this report, we present the results of a detailed study of the early stages of growth of $\text{Co}_3\text{O}_4/\alpha\text{-Al}_2\text{O}_3(0001)$ thin films, aiming at understanding the electronic and crystal surface structure of the interfacial oxide layer. We show, from x-ray photoelectron spectroscopy of the Co 2p edge, that the cobalt oxide growth begins with the formation of a Co^{3+} -rich interfacial layer, which we associate with the cobalt sesquioxide Co_2O_3 , crystalizing in the corundum structure.^{14,15}

This is a surprising result in that the cobalt sesquioxide, Co_2O_3 , is not the preferred cobalt oxide at the temperatures and pressures attainable in molecular beam epitaxy growth conditions. In fact, the electronic and catalytic properties of Co_2O_3 have not been studied extensively, possibly due to difficulties in synthesizing this compound. Chenavas et al.¹⁴ suggest the existence of a high pressure phase with low spin Co^{3+} ($a = 4.882$ Å, $c = 13.38$ Å) and a low pressure phase, with high spin Co^{3+} ($a = 4.782$ Å, $c = 12.96$ Å) based on the observation of a reduction in the unit cell volume upon annealing in air at 400°C for 30 min, where the spin state was inferred from the smaller ionic radius of high spin Co^{3+} . *Ab initio* (ground state) calculations for corundum Co_2O_3 suggest also that this oxide is energetically stable.¹⁶ The most stable oxides of cobalt include the high temperature rocksalt CoO (cobaltous oxide) phase, where the Co^{2+} ($S = 3/2$) occupy octahedral sites, and the mixed valence cobalt cobaltite, Co_3O_4 , crystalizing in the normal spinel structure ($a = 8.086$ Å)¹⁷ with the Co^{2+} occupying tetrahedral sites and the Co^{3+} occupying octahedral sites.^{18,19,20,21} The octahedral Co^{3+} ions are in a low spin state, $S = 0$, while the tetrahedral Co^{2+}

ions are in a high spin state ($S = 3/2$), which order antiferromagnetically below about 40 K.^{19,22}

II. EXPERIMENTAL

Film growth was carried out in an ultrahigh vacuum (UHV) oxide molecular beam epitaxy deposition system (base pressure of 1×10^{-9} mbar), using conditions identical to those reported earlier.^{10,11} Prior to film growth, the α - Al_2O_3 substrate was annealed at 600°C in UHV for 60 min, followed by exposure to atomic oxygen at 300°C for 30 min. This procedure results in α - Al_2O_3 (0001) surfaces free of carbon and yielding sharp reflection high energy electron diffraction (RHEED) and low energy electron diffraction (LEED) patterns, characteristic of atomically smooth surfaces (see Fig. 1 and Fig. 2). The only impurities detected by Auger electron spectroscopy (AES) consist of trace amounts of Ca (2%) and K (0.2%). Film growth was carried out at 300°C by simultaneous exposure of the substrate to an atomic Co beam evaporated thermally from an effusion cell and to an atomic oxygen beam generated by a magnetron plasma source; the O_2 partial pressure during growth was set to 3×10^{-5} mbar. The Co deposition rate was about 1 Å/min, as measured by a calibrated quartz thickness monitor. Growth rates were monitored before and after deposition throughout this study. The film growth was interrupted at several stages of the deposition process for LEED, AES and x-ray photoelectron spectroscopy (XPS) analysis, namely, after deposition of 1, 2, 10, 20 and 70 Å Co. From *ex situ* x-ray reflectometry of the film carried out after growth, the oxide film thickness was found to be 120 ± 10 Å, where the error bar includes possible systematic errors in the measurement. From this value, the corresponding cobalt oxide film thicknesses are obtained: 1.7, 3.4, 17, 34, and 120 Å. LEED, AES and XPS measurements were performed after transferring the sample under UHV from the growth chamber to a dedicated analysis chamber with a base pressure of 1×10^{-10} mbar; typical XPS measurement times ranged from 2-5 h. Before continuation of the film growth, the film surface was exposed to the atomic oxygen beam for 5 min with the sample held at 300°C. *Ex situ* x-ray diffraction (XRD) measurements were performed on the 120 Å film on a Shimadzu diffractometer operating in the parallel beam optics geometry.

III. RESULTS AND DISCUSSION

Film crystallinity was monitored during growth using RHEED, and the diffraction patterns after completion of each layer are shown in Fig. 1. As a general trend, the diffuse background scattering increased with increasing deposition thickness; the diffraction spots broadened with film thickness, starting with sharp patterns at low coverages (1.7, 3.4 Å), which became streakier at intermediate thicknesses (17, 34 Å) and spotty, transmission-

like, at larger thicknesses, in agreement with previous observations.¹¹ These results suggest that the cobalt oxide growth proceeds in the Stranski-Krastanov mode.²³

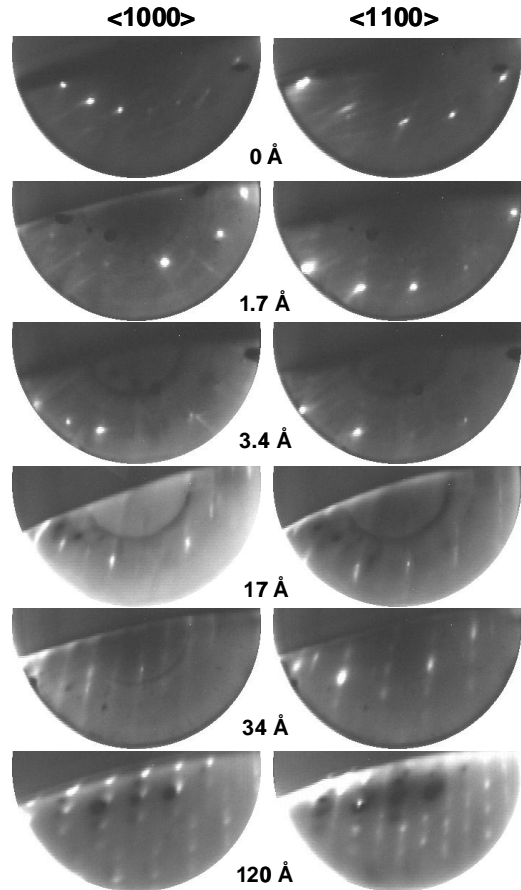


FIG. 1: RHEED patterns of the cobalt oxide film along two different azimuths of the α - Al_2O_3 (0001) surface at several stages of the film growth, as labeled. The incident electron beam energy is 15 keV.

LEED patterns taken at room temperature immediately after completion of each layer are shown in Fig. 2, showing (1×1) diffraction patterns whose overall features agree with the RHEED results. The oblique cell drawn in Fig. 2 (0 Å) corresponds to the α - Al_2O_3 (0001) unit cell (corundum, $a = 4.7570$ Å, $c = 12.9877$ Å in the hexagonal representation);^{24,25,26} the three-fold symmetric LEED pattern of the α - Al_2O_3 (0001) surface indicates that it is composed predominantly of double-layer atomic steps. The LEED pattern symmetry remains similar to that of the substrate up to 17 Å, while for 34 Å it starts resembling that of Co_3O_4 (111).^{11,27} This evolution in the LEED patterns can also be followed in Fig. 2(b), which shows the line profiles across the spots labeled A and B in Fig. 2. In order to correct for charging, slight differences in sample positioning, and for the different electron beam energies, the distance between these spots was normalized to the same value for all thicknesses. While for α - Al_2O_3 (0001) no features are present between these

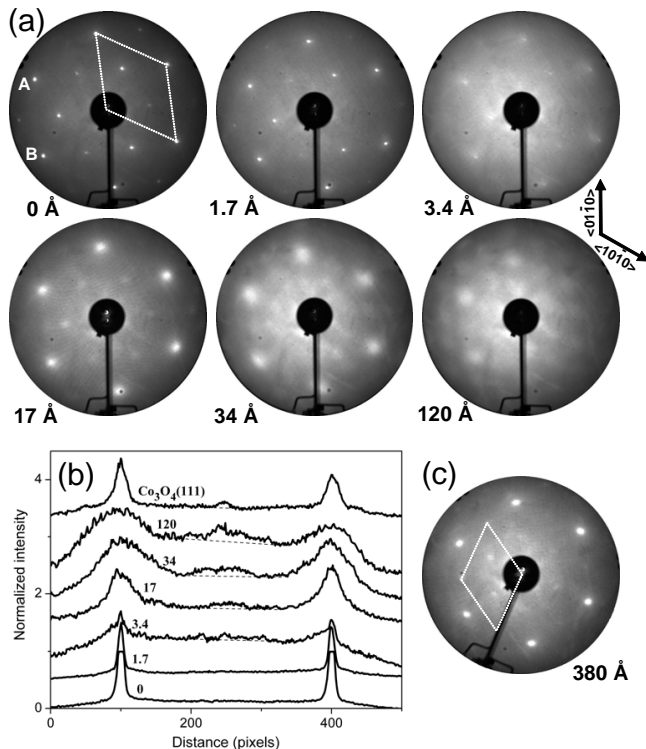


FIG. 2: (a) LEED patterns of the cobalt oxide film at several stages of film growth, as labeled. The incident electron beam energy is 100.0 eV for the patterns shown, except for the 34 Å (116.8 eV) and 120 Å films (138.2 eV). (b) LEED line profiles across the diffraction spots labeled A and B in (a) for the different cobalt oxide thickness; the profile for $\text{Co}_3\text{O}_4(111)$ corresponds to a LEED pattern of a 38 nm $\text{Co}_3\text{O}_4(111)/\alpha\text{-Al}_2\text{O}_3(0001)$ film annealed in air at 600°C for 14 h (104.3 eV), shown in (c). The dashed rhombus in (a) and (c) represent the LEED unit cells of $\alpha\text{-Al}_2\text{O}_3$ and Co_3O_4 , respectively.

spots, in $\text{Co}_3\text{O}_4(111)$ there is an intermediate diffraction spot, the presence of which can be used to identify the onset of this phase, at about 17 Å. The XRD measurements on the 120 Å film show the presence of the (hhh) planes of Co_3O_4 at the angle positions corresponding to the bulk values, indicating that the film is fully relaxed. The rocking curve around the (222) plane shows a single gaussian peak, with a width of 0.026° , which corresponds to a characteristic lengthscale in real space of about 180 nm.

Spectroscopic characterization by XPS and AES was performed for each layer thickness, but while XPS could be performed for all cobalt oxide thicknesses, AES could only be performed up to 17 Å, due to sample charging. The XPS spectra were obtained using the Mg K_α line ($h\nu = 1253.6$ eV) of a double anode x-ray source and a double pass cylinder mirror analyzer (PHI 15-255G) set at a pass energy of 25 eV (energy resolution of about 0.8 eV). The XPS data, acquired in energy steps of 0.05 eV, were smoothed using a 5-point adjacent averaging and corrected for the Mg K_α satellite. Charging is always a concern for insulating samples; one common method

of calibrating the energy scale against charging is to use the C 1s line from adventitious hydrocarbons,^{28,29} but this process cannot be used in these carbon-free samples. X-ray photoelectron emission charges the sample positively, while charging in (electron excited) AES may be of either sign, since the number of ejected electrons may be larger or smaller than the number of incident electrons (secondary electron emission, which is strongly energy dependent).^{30,31,32,33} Hence, comparing both the XPS and AES data can provide some information about the extent of charging.

To correct for sample charging in XPS, we consider the Auger and photoelectron spectral features of oxygen, namely, the O 1s peak and the KVV Auger and energy loss peaks, which lie near the Co 2p edge. We set the O 1s peak of $\alpha\text{-Al}_2\text{O}_3$ to the tabulated value of 531.5 eV,^{34,35} and the O 1s peak of the 120 Å film, expected to be representative of Co_3O_4 ,¹¹ to the tabulated value of 529.4 eV.^{36,37} For the 1.7 and 3.4 Å films, we assume that most of the O contribution to the photoelectron spectra arises from the substrate, and we tentatively set the O 1s peak to the same energy position as that of $\alpha\text{-Al}_2\text{O}_3$. We find that the KVV Auger loss peaks of O for these films also align with those for $\alpha\text{-Al}_2\text{O}_3$ and that the energy distance from the first O loss peak to the Co $2p_{3/2}$ is 15.9 eV for both 1.7 and 3.4 Å cobalt oxide films. For the thicker films, both first and second O Auger KVV loss peaks are visible, and shifted to much lower binding energies relative to the Co $2p_{3/2}$ peak, by 18.9 eV for the first O loss peak and by 5.6 eV for the second O loss peak for the 34 and 120 Å films; for the 17 Å film, the shift is slightly smaller, about 14.4 and 4.2 eV, respectively. Therefore, we can assign the O 1s peak to that of Co_3O_4 for the 34 and 17 Å films, although for the latter thickness the assignment is less certain. For reference, we also measured the XPS spectra of LaCoO_3 , where the Co cations are all trivalent; since LaCoO_3 is conducting at room temperature ($\sigma \sim 0.1 \Omega^{-1}\text{cm}^{-1}$),^{38,39} no charging is expected and no energy corrections have been applied to this XPS spectrum. The LaCoO_3 data are from a single crystal wafer cut along one pseudo-cubic (110) plane (mechanically polished to optical flatness and annealed in air at 600°C for 67.5 hours), and were acquired after cleaning *in situ* in oxygen plasma at 300°C for 30 min. The LaCoO_3 single crystal, grown using the floating zone method,⁴⁰ is twinned, as shown by Laue and x-ray diffraction, but is otherwise well ordered. The shoulder on the O 1s peak, which was very prominent in the XPS spectra of the sample as-inserted to the analysis system, is due to adsorbed hydroxyl groups that remain on the surface.⁴¹ The XPS spectra for all samples thus calibrated are shown in Fig. 3.

Three distinct features in the XPS spectra as a function of cobalt oxide thickness are apparent: (i) the energy difference between the $2p_{1/2}$ and $2p_{3/2}$ peaks remains constant at 15.2 eV with increasing cobalt oxide thickness, and between Co_3O_4 , LaCoO_3 , and CoO ;³⁷ the energy difference between multiplets is sometimes employed to ascertain the ionic valence state, but is not suitable for

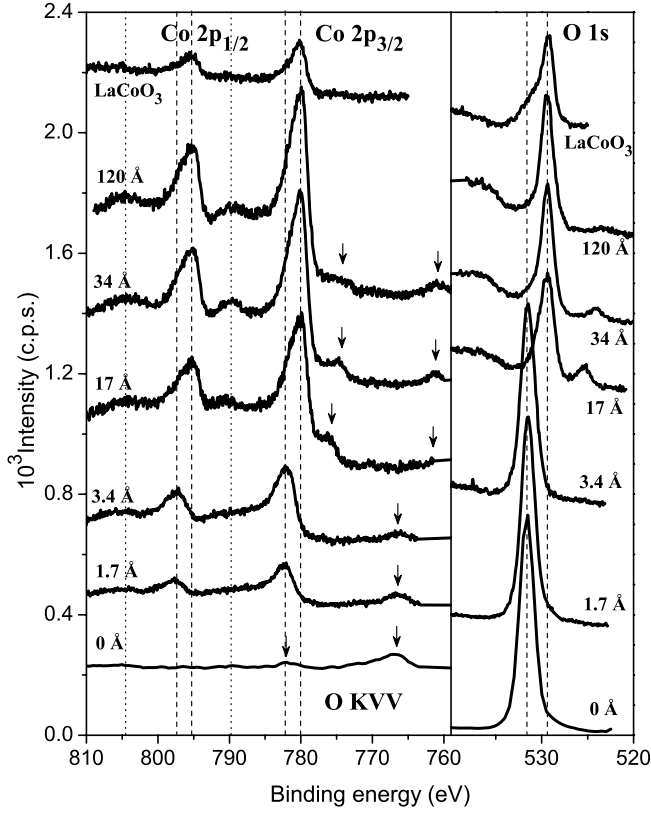


FIG. 3: XPS spectra as a function of cobalt oxide film thickness at the Co 2p and O 1s edges. Arrows indicate the energy position of the O KVV loss peaks, dashed lines indicate main peak positions, and dotted lines indicated the energy position of the Co_3O_4 satellite peaks. Data have been shifted vertically for convenient display.

discriminating these different cobalt oxide compounds. (ii) The higher Co 2p binding energies observed for the 1.7 and 3.4 Å cobalt oxide films track the change in the binding energy of the O 1s peak; this energy shift is thus attributed to band bending effects (pinning of the Fermi level to that of the $\alpha\text{-Al}_2\text{O}_3$ substrate) rather than to a true chemical shift. This agrees with the fact that for the thinner films (1.7 and 3.4 Å) we find no splitting or broadening in the O 1s peak, as shown in Fig. 4; the slightly larger peak width in the O 1s line at 17 Å could be the result of a small contribution from the substrate O 1s peak at 531.5 eV. At this thickness, the substrate contribution becomes very small, as is shown by the fact that the Al 2p and 2s lines can no longer be detected in the XPS survey scans (the latter have lower counting statistics than in the fine Co 2p and O 1s edge energy scans, where a small contribution may be present). (iii) Significantly, we note the absence of satellite peaks in the Co 2p spectra of the 1.7 and 3.4 Å films, and the appearance of weak satellite peaks, characteristic of Co_3O_4 ,^{36,42,43,44} at larger thicknesses. At 17 Å, the satellite peaks are still strongly suppressed and lie at slightly higher binding energies compared to the thicker cobalt oxide films. This

shows that the 1.7 and 3.4 Å films behave spectroscopically (and electronically) very differently from the thicker (Co_3O_4) films, pointing to a transition from an interfacial cobalt oxide layer to bulk-like Co_3O_4 at around 17 Å.

The presence and energy position of satellite peaks in the core and valence levels of the photoelectron spectra of the 3d transition metal oxides depend strongly on the ionic environment, cation valency, and electron occupancy.^{45,46,47,48,49,50} These satellite peaks arise as a consequence of the fact that several channels are available that compete for the final (excited) state. In 2p core level photoelectron emission, the presence of the core-hole leads to strong modifications in the energy landscape of the cation and anion (ligand) orbitals that favor screening of the core hole via charge transfer from *sp* or ligand orbitals. Two processes compete for the final state, one corresponding to the case where charge is transferred from the ligand to the 3d orbital, effectively screening the core hole, which is usually associated with the main line (*well screened* state, represented by $|2p^5 3d^{n+1} \underline{L}\rangle$, where \underline{L} represents the ligand hole).^{51,52,53,54,55,56} The other competing process corresponds to a less well screened state (with higher apparent binding energy), where no charge transfer from the ligand takes place and where charge compensation is provided by *sp* orbitals (*unscreened* state, represented by $|2p^5 3d^n\rangle$). In a simplified cluster model,^{51,52,53,54,55} the photoemission process is treated as a scattering event from an initial hybridized state

$$|\psi_g\rangle = \alpha_0 |2p^6 3d^n\rangle + \alpha_1 |2p^6 3d^{n+1} \underline{L}\rangle + \dots \quad (1)$$

to final hybridized states of the form:

$$|\psi_f\rangle = \beta_0 |2p^5 3d^n\rangle + \beta_1 |2p^5 3d^{n+1} \underline{L}\rangle + \dots \quad (2)$$

The final state with the lowest energy is associated with the main 2p photoelectron line, while the other higher energy states give rise to the satellite lines, although in all cases a strong mixture of orbital states may be present. In particular, for the case of a filled 3d shell ($n = 10$, as in Cu_2O), charge transfer to the 3d orbital is precluded, and the final state is dominated by the *sp*-screened state, $|5p^5 3d^{10}\rangle$, with no satellite peaks.⁵⁵ In addition, multiplet splitting of the final states due to exchange interaction with the core hole may introduce further features in the spectra.^{47,49,50,53,55,57,58,59} Strong satellite structures occur predominantly in transition-metal and rare-earth cations, and it is generally accepted that charge transfer peaks give the most intense contribution, while multiplet splitting adds to the fine structure, although separation between these contributions is sometimes difficult.^{47,49,50,57,60}

For our purposes, we are interested in the satellite features that may allow us to identify the ionic state of the cobalt cations, particularly at small cobalt oxide thicknesses, where no satellites are observed. In a simplified relaxation model, the absence of satellite features can be

understood as a consequence of an electronic structure consisting of filled valence levels to which charge transfer from the ligand is precluded.^{49,55,61} This is expected to be the case for octahedrally coordinated trivalent cobalt, where the crystal field splits the 3d levels into a low energy triplet t_{2g} level, and to a high energy e_g doublet, leading to full occupancy of the t_{2g} states, with a correspondingly low spin state ($S = 0$);^{19,44,62} one example where this occurs is in LaCoO_3 , whose Co 2p XPS spectrum is shown in Fig. 3. In cluster theory language, this corresponds to the situation where the charge transfer energy Δ (difference between the excited $|2p^6 3d^7 \underline{L}\rangle$ and ground $|2p^6 3d^6\rangle$ initial states of the neutral atom), is larger than the core-hole-d-electron Coulomb energy, Q , such that the screened $|2p^5 3d^7 \underline{L}\rangle$ final state remains higher in energy than, and little hybridized with, the unscreened $|2p^5 3d^7 \underline{L}\rangle$ state.^{53,54,55} A similar situation occurring in Fe^{2+} compounds has been analyzed by Kroll *et al.*⁶¹ Hence, in Co_3O_4 , the strongly suppressed satellite peak is explained by the fact that the octahedrally coordinated Co^{3+} states do not contribute to charge transfer and therefore to shake-up processes; the remaining 1/3 Co cations are tetrahedrally coordinated Co^{2+} and give rise to shake-up peaks, since the crystal field now leads to a low energy e_g doublet and a partially filled higher energy t_{2g} triplet.^{19,62} A comparison of the binding energies of the 2p Co edge peaks for several cobalt oxide compounds (Table I, where we excluded mixed valency oxides other than Co_3O_4) supports the view that these satellite features may be employed to identify the valence state of cobalt in oxides,^{48,63,64,65} although exceptions are apparent, including the presence of (strongly suppressed) satellite peaks in the layered LiCoO_2 (where the Co^{3+} occupy octahedral sites).^{66,67,68} For the listed spinels where Co^{2+} occupy tetrahedral sites, CoAl_2O_4 , CoCr_2O_4 , and the tetragonal CoMn_2O_4 (stable only at elevated temperatures with parasite phases, including MnCo_2O_4 , known to develop at ambient temperatures),⁶⁹ the satellite peak splitting is similar to that of divalent cobalt in an octahedral environment, and here Co_3O_4 seems to be the outlier.

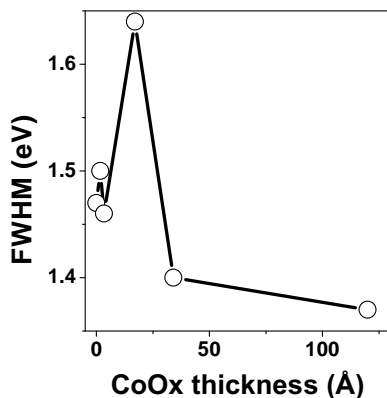


FIG. 4: Variation of the O 1s XPS peak full width at half maximum (FWHM) as a function of cobalt oxide thickness.

TABLE I: Binding energy (B.E.) and satellite peak splitting (S.S.) of the Co 2p peaks for selected cobalt oxide compounds, in eV. The second column refers to the crystal field environment, octahedral (o) or tetrahedral (t), while the third column indicates the formal valence state of the Co cation. [*] This work.

Oxide	Site	Ion	2p _{3/2}		2p _{1/2}		Ref.
			B.E.	S.S.	BE.	S.S.	
CoO	o	2+	780.5	5.9	796.3	6.7	[36]
CoFe ₂ O ₄	o	2+	780.6	5.1	796.2	6.5	[70]
CoFe ₂ O ₄	o	2+	779.9	6.2	795.7	6.2	[64]
LaCoO ₃	o	3+	780.1	—	795.3	—	[*]
CuCoMnO ₄	o	3+	780.0	—	795.0	—	[48]
Co ₃ O ₄	o	3+	779.6	—	794.5	—	[36]
MnCoZnO ₄	o	3+	780.4	—	795.4	—	[48]
LiCoO ₂	o	3+	779.5	10.6	794.6	9.5	[66,68]
CoAl ₂ O ₄	t	2+	781.0	5.0	796.7	6.3	[64]
CoCr ₂ O ₄	t	2+	780.4	5.3	796.3	6.2	[64]
CoMn ₂ O ₄	t	2+	780.2	5.6	796.3	6.5	[48,64]
Co ₃ O ₄	t	2+	780.7	8.8	796.0	8.5	[36]

The case of Co^{3+} in a tetrahedral environment should also give rise to charge-transfer satellite peaks, since in such a crystal field both the low energy e_g doublet and the higher energy t_{2g} triplet have empty states.^{19,62} These observations suggest that the interfacial oxide layer present at low cobalt oxide thicknesses consist of octahedrally coordinated Co^{3+} cations. We envisage two possibilities that can explain this result: it either corresponds to a fully oxidized cobalt compound with a corundum structure, Co_2O_3 , where all cations are (slightly distorted) octahedrally coordinated; or to the octahedrally coordinated Co^{3+} layer in the $\text{Co}_3\text{O}_4(111)$ structure, which also would initiate the spinel growth along the [111] direction. The LEED and RHEED patterns for the 1.7 and 3.4 Å films, similar to those of the $\alpha\text{-Al}_2\text{O}_3$ substrate, seem to support the first interpretation of the spectroscopy data.

Is it now well established that under the preparation conditions used here, the $\alpha\text{-Al}_2\text{O}_3(0001)$ surface is the non-polar, (1×1) Al-terminated surface.^{71,72,73,74,75,76} During Co deposition, the cobalt oxide layer is expected to continue the $\alpha\text{-Al}_2\text{O}_3$ close-packed oxygen sublattice, with either the [AB]A or [AB]C stacking sequences, where the square brackets enclose the hcp stacking of the $\alpha\text{-Al}_2\text{O}_3$ O sublattice. The first stacking sequence is a continuation of the hcp stacking and contains octahedral interstitial sites only, while the second stacking sequence also contains tetrahedral sites and is expected to mark the onset of the spinel crystal structure. Based on the LEED and XPS results, and considering the atomic configurations expected for the available cationic interstitial sites in the close-packed O sublattice, we propose next a model to explain the epitaxial relationships observed in the spinel(111)/ $\alpha\text{-Al}_2\text{O}_3(0001)$ system. In this model, the transition from the corundum to the spinel structure can occur in two possible ways, schematically shown in Fig. 5. Starting with the stoichiometric corundum (0001) surface, Fig. 5(a), (i) the Co cations oc-

cupy non-corundum octahedral sites concomitant with the initiation of the fcc stacking of the O sublattice, forming the octahedral Co^{3+} layer of the $\text{Co}_3\text{O}_4(111)$ structure, Fig. 5(b); or (ii) the Co cations occupy both corundum sites (which are tetrahedrally coordinated in the fcc stacking of the O sublattice), and octahedral and tetrahedral non-corundum sites to form the mixed valence Co^{2+} - Co^{3+} - Co^{2+} layer of $\text{Co}_3\text{O}_4(111)$, as shown in Fig. 5(c). Hence, one finds that the spinel structure can very naturally continue the corundum structure without causing undue violence to the cationic distribution at the interface between the two crystal structures. The different possible ways in which the spinel structure can be generated, and the different equivalent, but not identical, planes that form the Co_3O_4 unit cell along the $[111]$ direction, imply that the presence of stacking faults and antiphase boundaries are very likely. They may be responsible, in part, for the surface disorder observed in the RHEED and LEED patterns.

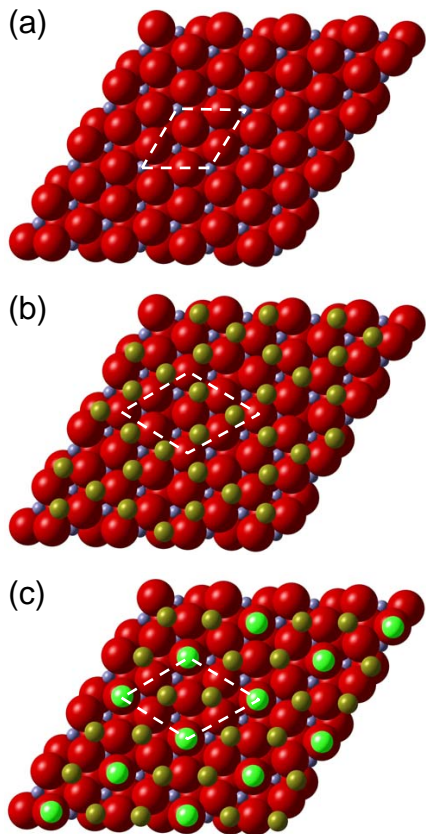


FIG. 5: (a) Atomic structure of the stoichiometric corundum (0001) surface. (b) Model for the epitaxial growth of the $\text{Co}_3\text{O}_4(111)$ structure on the corundum (0001) surface, showing the formation of the octahedral Co^{3+} layer. (c) Alternative growth model, showing the formation of the mixed valence tetrahedral Co^{2+} -octahedral Co^{3+} -tetrahedral Co^{2+} layer of $\text{Co}_3\text{O}_4(111)$ on the corundum (0001) surface. For each surface, the dashed area indicates the primitive surface unit cell.

We can, therefore, reconstruct the most likely growth

process in the $\text{Co}_3\text{O}_4/\alpha\text{-Al}_2\text{O}_3(0001)$ system. We assume in the following that one unit layer corresponds to the separation between planes of the close-packed O sublattice, of about 2.3 Å, using the lattice parameter of Co_3O_4 . In broad terms, we envisage the cobalt oxide film growth as follows. At the earliest stage of growth, Co cations fill the empty octahedral corundum sites of the non-polar $\alpha\text{-Al}_2\text{O}_3(0001)$ surface, resulting in a corundum-like layer composed of half Al^{3+} cations and half Co^{3+} cations. At 3.4 Å, the cobalt oxide film corresponds to about 1.5 atomic layers, and the observation of octahedrally coordinated Co^{3+} cations in XPS at this thickness could result from the formation of the octahedrally coordinated plane of Co_3O_4 upon the onset of the oxygen C layer of the fcc stacking. However, the LEED patterns show no evidence for the formation of the spinel (111) surface up to about 17 Å. Hence, we conclude that the cobalt oxide film continues with the corundum structure up to at least 2-3 atomic layers, forming effectively an interfacial cobalt sesquioxide layer, mediating the transition between the sapphire and spinel structures. We do not observe surface reconstructions (LEED, RHEED) or changes in valency of the Co cations (XPS) during the initial stages of growth; this may be expected if the corundum structure grows in Co-O₃-Co layer units, which are charge compensated. Since the Co_2O_3 phase is not thermodynamically the most stable phase, the Co_3O_4 phase eventually sets in, with the transition occurring as described in the model above. This is observed to occur at 17 Å, where the XPS shows the presence of tetrahedral Co cations, characteristic of the spinel $\text{Co}_3\text{O}_4(111)$ structure.

IV. CONCLUSIONS

We have studied in detail the early growth stages of epitaxial $\text{Co}_3\text{O}_4(111)$ films grown on $\alpha\text{-Al}_2\text{O}_3(0001)$ single crystals. The RHEED and LEED results show that film growth proceeds via the Stranski-Krastanov mode; the electron diffraction data, in combination with spectroscopic characterization by XPS, indicate the formation of an octahedrally coordinated, fully oxidized, interfacial cobalt oxide film that mediates the transition between the corundum and the spinel crystal structures. These results are a telling example of the strongly modified structural and electronic properties of metal oxides that are induced by the change in crystal symmetries at interfaces.

Acknowledgments

The authors acknowledge financial support by the NSF through MRSEC DMR 0520495 (CRISP), and by the US DOE Basic Energy Sciences Grants DEFG02-98ER14882 and DEFG02-06ER15834. The surface crystal structures were produced with the aid of the DL Visualize public software.⁷⁷

-
- * Corresponding author. Email: carlos.vaz@yale.edu
- ¹ V. E. Henrich and P. A. Cox, *The surface science of metal oxides* (Cambridge University Press, Cambridge, 1994).
 - ² C. Noguera, J. Phys.: Condens. Matter **12**, R367 (2000).
 - ³ J. Goniakowski, F. Finocchi, and C. Noguera, Rep. Prog. Phys. **71**, 016501 (2008).
 - ⁴ W. A. Harrison, E. A. Kraut, J. R. Waldrop, and R. W. Grant, Phys. Rev. B **18**, 4402 (1978).
 - ⁵ P. W. Tasker, J. Phys. C: Solid State Phys. **12**, 4977 (1979).
 - ⁶ M. Ritter and W. Weiss, Surf. Sci. **432**, 81 (1999).
 - ⁷ M. Gajdardziska-Josifovska, R. Plass, M. A. Schofield, D. R. Giese, and R. Sharma, J. Electron Microsc. **51**, S13 (2002).
 - ⁸ V. K. Lazarov, R. Plass, H.-C. Poon, D. K. Saldin, M. Weinert, S. A. Chambers, and M. Gajdardziska-Josifovska, Phys. Rev. B **71**, 115434 (2005).
 - ⁹ W. Meyer, K. Biedermann, M. Gubo, L. Hammer, and K. Heinz, J. Phys.: Condens. Matter **20**, 265011 (2008).
 - ¹⁰ C. A. F. Vaz, H.-Q. Wang, C. H. Ahn, V. E. Henrich, M. Z. Baykara, T. Schwendemann, N. Pilet, B. J. Albers, U. Schwarz, L. H. Zhang, et al., Surf. Sci. **603**, 291 (2009).
 - ¹¹ C. A. F. Vaz, V. E. Henrich, C. H. Ahn, and E. I. Altman, Journal of Crystal Growth **311**, 2648 (2009).
 - ¹² U. Schwingenschlögl and C. Schuster, Europhys. Lett. **81**, 17007 (2008).
 - ¹³ H. Chen, A. M. Kolpak, and S. Ismail-Beigi, Phys. Rev. B **79**, 161402(R) (2009).
 - ¹⁴ J. Chenavas, J. C. Joubert, and M. Marezio, Solid State Commun. **9**, 1057 (1971).
 - ¹⁵ G. V. Samsonov, ed., *The oxide handbook* (IFI/Plenum, New York, 1982), 2nd ed.
 - ¹⁶ M. Catti and G. Sandrone, Faraday Discuss. **106**, 189 (1997).
 - ¹⁷ J. P. Picard, G. Baud, J. P. Besse, and R. Chevalier, Journal of the Less-Common Metals **75**, 99 (1980).
 - ¹⁸ P. Cossee, Journal of Inorganic and Nuclear Chemistry **8**, 483 (1958).
 - ¹⁹ W. L. Roth, J. Phys. Chem. Solids **25**, 1 (1964).
 - ²⁰ W. L. Smith and A. D. Hobson, Acta Cryst. B **29**, 362 (1973).
 - ²¹ M. Iliev, S. Angelov, I. Z. Kostadinov, V. Bojchev, and V. Hadjiev, Phys. Stat. Sol. (a) **71**, 627 (1982).
 - ²² D. Scheerlinck and S. Hautecler, Phys. Stat. Sol. (b) **73**, 223 (1976).
 - ²³ J. A. Venables, G. D. Spiller, and M. Handbücken, Rep. Prog. Phys. **47**, 399 (1984).
 - ²⁴ R. E. Newnham and Y. M. de Haan, Zeitschrift für Kristallographie **117**, 235 (1962).
 - ²⁵ C. S. G. Cousins, J. Phys. C: Solid State Phys. **14**, 1585 (1981).
 - ²⁶ A. Kirfel and K. Eichhorn, Acta Cryst. A **46**, 271 (1990).
 - ²⁷ S. C. Petitto, E. M. Marsh, G. A. Carson, and M. A. Langell, J. Molecular Catalysis A: Chemical **281**, 49 (2008).
 - ²⁸ F. Cordier and E. Ollivier, Surf. Interface Anal. **23**, 601 (1995).
 - ²⁹ M. R. Alexander, G. E. Thompson, and G. Beamson, Surf. Interface Anal. **29**, 468 (2000).
 - ³⁰ V. E. Henrich, Rev. Sci. Instrum. **44**, 456 (1973).
 - ³¹ N. R. Rajopadhye, V. A. Joglekar, V. N. Bhoraskar, and S. V. Bhoraskar, Sol. State Commun. **60**, 675 (1986).
 - ³² M. P. Seah and S. J. Spencer, J. Electron Spectrosc. Relat. Phenom. **109**, 291 (2000).
 - ³³ E. I. Rau, S. Fakhfakh, M. V. Andrianov, E. N. Evstafeva, O. Jbara, S. Rondot, and D. Mouze, Nucl. Instr. and Meth. in Phys. Res. B **266**, 719 (2008).
 - ³⁴ C. D. Wagner, W. M. Riggs, L. E. Davis, J. F. Moulder, and G. E. Muilenberg, eds., *Handbook of x-ray photoelectron spectroscopy* (Perkin-Elmer Corporation, Eden Prairie, Minnesota, 1979).
 - ³⁵ S. P. Chenakin, R. P. Silvy, and N. Kruse, J. Phys. Chem. B **109**, 14611 (2005).
 - ³⁶ T. J. Chuang, C. R. Brundle, and D. W. Rice, Surf. Sci. **59**, 413 (1976).
 - ³⁷ S. C. Petitto and M. A. Langell, J. Vac. Sci. Technol. A **22**, 1690 (2004).
 - ³⁸ P. Dordor, S. Joiret, J. P. Doumercj, J. C. Launayj, J. Claverie, and P. Hagenmüller, Phys. Stat. Sol. (a) **93**, 321 (1986).
 - ³⁹ Z. Jiráč, J. Hejtmánek, K. Knížek, and M. Veverka, Phys. Rev. B **78**, 014432 (2008).
 - ⁴⁰ D. Prabhakaran, A. T. Boothroyd, F. R. Wondre, and T. J. Prior, J. Cryst. Growth **275**, e827 (2005).
 - ⁴¹ J. Haber, J. Stoch, and L. Ungier, J. Electron Spectrosc. Relat. Phenom. **9**, 459 (1976).
 - ⁴² J. Haber and L. Ungier, J. Electron Spectrosc. Relat. Phenom. **12**, 305 (1977).
 - ⁴³ M. A. Langell, M. D. Anderson, G. A. Carson, L. Peng, and S. Smith, Phys. Rev. B **59**, 4791 (1999).
 - ⁴⁴ H. A. Hagelin-Weaver, G. B. Hoflund, D. M. Minahan, and G. N. Salaita, Appl. Surf. Sci. **235**, 420 (2004).
 - ⁴⁵ D. C. Frost, C. A. McDowell, and I. S. Woolsey, Mol. Phys. **27**, 1473 (1974).
 - ⁴⁶ K. S. Kim and N. Winograd, Chem. Phys. Lett. **31**, 312 (1975).
 - ⁴⁷ G. A. Vernon, G. Stucky, and T. A. Carlson, Inorg. Chem. **15**, 278 (1976).
 - ⁴⁸ V. A. M. Brabers and F. van Setten, J. Phys. D: Appl. Phys. **16**, L169 (1983).
 - ⁴⁹ B. W. Veal and A. P. Paulikas, Phys. Rev. B **31**, 5399 (1985).
 - ⁵⁰ B. Mayer, S. Uhlenbrock, and M. Neumann, J. Electron Spectrosc. Relat. Phenom. **81**, 63 (1996).
 - ⁵¹ S. Larsson, Chem. Phys. Lett. **40**, 362 (1976).
 - ⁵² S. Larsson and M. Braga, Chem. Phys. Lett. **48**, 596 (1977).
 - ⁵³ G. van der Laan, C. Westra, C. Haas, and G. A. Sawatzky, Phys. Rev. B **23**, 4369 (1981).
 - ⁵⁴ J. Zaanen, C. Westra, and G. A. Sawatzky, Phys. Rev. B **33**, 8060 (1986).
 - ⁵⁵ J. Ghijsen, L. H. Tjeng, J. van Elp, H. Eskes, J. Westerink, G. A. Sawatzky, and M. T. Czyzyk, Phys. Rev. B **38**, 11322 (1988).
 - ⁵⁶ A. Fujimori, in *Core-Level Spectroscopy in Condensed Systems*, edited by J. Kanamori and A. Kotani (Springer-Verlag, Berlin, 1987), p. 136.
 - ⁵⁷ A. Rosencwaig, G. K. Wertheim, and H. J. Guggenheim, Phys. Rev. Lett. **27**, 479 (1971).
 - ⁵⁸ K. Okada, A. Kotani, and B. T. Thole, J. Electron Spectrosc. Relat. Phenom. **58**, 325 (1992).
 - ⁵⁹ S. Hüfner, *Photoelectron Spectroscopy* (Springer-Verlag, Berlin, 2003), 2nd ed.

- ⁶⁰ S. Hüfner, in *Photoemission in Solids II*, edited by L. Ley and M. Cardona (Springer-Verlag, Berlin, 1979), no. 27 in Topics in Applied Physics, p. 173.
- ⁶¹ T. Kroll, F. Roth, A. Koitzsch, R. Kraus, D. R. Batchelor, J. Werner, G. Behr, B. Büchner, and M. Knupfer, *New Journal of Physics* **11**, 025019 (2009).
- ⁶² J. B. Goodenough, *Progress in Solid State Chemistry* **5**, 145 (1971).
- ⁶³ J. P. Bonnelle, J. Grimblot, and A. D’Huysser, *J. Electron Spectrosc. Relat. Phenom.* **7**, 151 (1975).
- ⁶⁴ M. Oku and K. Hirokawa, *J. Electron Spectrosc. Relat. Phenom.* **8**, 475 (1976).
- ⁶⁵ S. Laureti, E. Agostinelli, G. Scavia, G. Varvaro, V. R. Albertini, A. Generosi, B. Paci, A. Mezzi, and S. Kaciulis, *Applied Surface Science* **254**, 5111 (2008).
- ⁶⁶ M. Oku, *J. Solid State Chem.* **23**, 177 (1978).
- ⁶⁷ J. P. Kemp and P. A. Cox, *J. Phys.: Condens. Matter* **2**, 9653 (1990).
- ⁶⁸ A. W. Moses, G. G. Flores, J.-G. Kim, and M. A. Langell, *Appl. Surf. Sci.* **253**, 4782 (2007).
- ⁶⁹ R. Buhl, *J. Phys. Chem. Solids* **30**, 805 (1969).
- ⁷⁰ Z. Gu, X. Xiang, G. Fan, and F. Li, *J. Phys. Chem. C* **112**, 18459 (2008).
- ⁷¹ I. Manassidis, A. D. Vita, and M. Gillan, *Surf. Sci. Lett.* **285**, L517 (1993).
- ⁷² J. Ahn and J. Rabalais, *Surf. Sci.* **388**, 121 (1997).
- ⁷³ G. Renaud, *Surface Science Reports* **32**, 5 (1998).
- ⁷⁴ E. A. A. Jarvis and E. A. Carter, *J. Phys. Chem. B* **105**, 4045 (2001).
- ⁷⁵ E. Wallin, J. M. Andersson, E. P. Münger, V. Chirita, and U. Helmersson, *Phys. Rev. B* **74**, 125409 (2006).
- ⁷⁶ P. Guénard, G. Renaud, A. Barbier, and M. Gautier-Soyer, *Surf. Rev. Lett.* **5**, 321 (1998).
- ⁷⁷ B. G. Searle, *Comput. Phys. Commun.* **137**, 25 (2001).